

**DOSIMETRIC STUDY OF GENIPIN GELATIN-
CHEMICAL ADDITIVES POLYMER GEL USING 6 MV
AND 10 MV THERAPEUTIC FACILITIES**

AMER MAHMOUD MOHAMMAD ALJARRAH

UNIVERSITI SAINS MALAYSIA

2015

**DOSIMETRIC STUDY OF GENIPIN GELATIN-
CHEMICAL ADDITIVES POLYMER GEL USING 6 MV
AND 10 MV THERAPEUTIC FACILITIES**

by

AMER MAHMOUD MOHAMMAD ALJARRAH

Thesis submitted in fulfillment of the requirements

for the degree of

Doctor of Philosophy

May 2015

ACKNOWLEDGMENT

In the name of Allah, The Most Gracious and Most Merciful, I am truly grateful to Allah, the most beneficent and the most merciful, for granting me health, patience, and strength throughout my research to complete it successfully in difficult times. I prayed for His kindness and forgiveness in our lives and hereafter.

I thank my supervisor, Dr. Azhar Abdul Rahman, School of Physics, Universiti Sains Malaysia (USM) for giving me the opportunity to work with him, for providing a comfortable, friendly, and enjoyable work environment, for being patient, for understanding and cooperation in difficult times, for his valuable instructions, and for encouraging and guiding me in our research problems. I am grateful in every possible way and hope to keep our collaboration in the future.

I gratefully acknowledge my co-supervisor, Dr. Iskandar Shahrin Mustafa, School of Physics, USM, for his advice, expertise, support, and helpful suggestions. I would also like to express my gratitude to the Medical Imaging Unit of Mount Mariam Cancer Hospital, Penang, Malaysia, for providing me great facilities during my research. I also wish to give my special thanks to the School of Physics of USM for those who taught me there, especially Prof. Mohamad Suhaimi Jaafar, Prof. Sohail Aziz, Prof. Abdul Aziz Tajuddin, and Prof. Sivamany Kandaiya. My gratitude also goes to all my friends and our laboratory technicians and staff for their cooperation and assistance to complete this work.

Special thanks also go to Dr. Nur Ashikin for her help and suggestions during this work. My sincere thanks also go to the School of Chemistry at USM for their assistance, especially to Prof. Bahruddin and for my colleagues Marwan Shalash,

Baleeq and Baker for the wonderful guide, as well as to Dr. Ahmad Makahleh and Dr. Samer Atawneh for their invaluable cooperation and timely help in the study.

On a personal note, my parents are the sole reason for my education. I want to acknowledge my father for sending all his children to school on limited resources and difficult times. I also owe much thanks to my mother for her sacrifices and prayers through the course of my life. I acknowledge her for always reminding me that time is too precious to waste and for wishing nothing but education for all her children. I am also thankful to my sisters and my brothers for their prayers, support, and good wishes. Finally, I want to acknowledge my wife and my lovely kids Mohamed, Mallak, Shima, Rima, and Hesham. I do not have appropriate words to weigh their encouragement, cooperation, patience, and understanding to achieve my goals to finish my work.

TABLE OF CONTENTS

	PAGE
ACKNOWLEDGMENT	II
TABLE OF CONTENTS	IV
LIST OF TABLES	VIII
LIST OF FIGURES	X
LIST OF ABBREVIATIONS	XIV
LIST OF SYMBOLS	XVI
LIST OF PUBLICATIONS	XVII
ABSTRAK	XVIII
ABSTRACT	XX
CHAPTER 1 INTRODUCTION	1
1.1 Background.....	1
1.2 Motivation for a 3D Dosimeter.....	4
1.3 Genipin Gel Dosimeter	6
1.4 Gold Nanoparticles (AuNPs) in Radiotherapy	7
1.5 Problem Statement.....	9
1.6 Significance of Study.....	10
1.7 Objectives of the Study.....	11
1.8 Scope of Research.....	11
1.9 Thesis Outline.....	12
CHAPTER 2 THEORETICAL BACKGROUND AND LITERATURE REVIEW	14
2.1 Main Interactions of Photons with Matter	14
2.1.1 Photoelectric Effect	15
2.1.2 Rayleigh (Coherent) Scattering	16
2.1.3 Compton Scatter (Incoherent Scatter)	17
2.1.4 Pair Production	18
2.2 Production of X-Rays	19
2.2.1 X-Ray Tubes.....	20
2.2.2 Characteristic X-Ray Spectrum	21
2.2.3 Bremsstrahlung Spectrum.....	22
2.3 X-Ray Attenuation.....	23

2.3.1	Linear Attenuation Coefficient	23
2.3.2	Mass Attenuation Coefficient	25
2.4	External Photon Beam Radiotherapy.....	26
2.4.1	Radiation Absorbed Dose	27
2.4.2	Photon Beam Dose Distribution	28
2.4.2.1	Off -axis Beam Profile and Uniformity.....	28
2.4.2.2	Central-axis Depth Dose	30
2.4.2.3	Tissue-Phantom Ratio	31
2.5	Polymer Gel Dosimeters.....	32
2.5.1	History and development.....	32
2.5.2	Formulation and Main Additives.....	35
2.5.3	Dose Enhancement Using Polymer Gel	40
2.5.4	Applications and Limitations.....	42
2.6	Properties of Polymer Gel Dosimeters	44
2.6.1	Visible Absorption Dose Response	45
2.6.2	Stability.....	48
2.6.3	Temperature Dependence	49
2.6.4	Uncertainty Measurements	49
2.6.5	Uncertainty in Dose Measurement and Dose Resolution	50
2.6.6	Water Equivalence.....	52
2.6.6.1	Calculations of Effective Atomic Number and Electron Density	53
2.6.6.2	Linear Attenuation Coefficient Measurements	54
2.7	Evaluation Techniques.....	55
2.8	Density and CT Number	56
2.9	Clinical Radiotherapy Validations in 3D.....	57
CHAPTER 3 METHODOLOGY		60
3.1	Gel Dosimetry Technique Overview	60
3.2	Genipin Gel Formulation.....	62
3.2.1	Chemical Ingredients	62
3.2.2	Genipin Gel Preparation	62
3.2.3	Chemical Additives	64
3.2.3.1	Inorganic Salt	64
3.2.3.2	Glucose.....	64
3.2.3.3	Gold Nanoparticles AuNPs	65
3.3	Dosimetric Equipment	66

3.3.1	Phantoms and Containers	66
3.3.1.1	Gel Containers.....	66
3.3.1.2	Solid Water Phantom	66
3.3.1.3	Perspex Phantoms	68
3.3.1.4	Water Phantom.....	69
3.3.2	Ionization Chamber	69
3.3.3	Radiochromic Film (EBT3).....	70
3.4	Radiation Devices and Apparatus.....	71
3.4.1	Medical Linear Accelerator (LINAC)	71
3.4.2	Narrow Beam Geometry.....	72
3.5	Irradiation Techniques	75
3.5.1	Calibration Curve	75
3.5.1.1	Polymer Gel	75
3.5.1.2	Radiochromic Film.....	77
3.5.2	Dosimetric Characteristics of Therapeutic Photon Beams	78
3.5.2.1	Beam Profile and Uniformity.....	79
3.5.2.2	The Percentage Depth Dose	81
3.6	Evaluation Techniques of Genipin Gel Dosimeter	83
3.6.1	Computed Tomography (CT)	83
3.6.2	Epson Perfection V700 Scanner	85
3.6.3	UV-VIS Spectrophotometry	86
3.7	Visible Absorption Dose Response	88
3.8	Temporal Stability Measurements of Genipin Gel Dosimeter	88
3.8.1	Pre-irradiation Temporal Stability Measurements.....	89
3.8.2	Post-Irradiation Temporal Stability Measurements	90
3.8.3	Reproducibility of Genipin Gel Dosimeter.....	90
3.9	Techniques for Determining Genipin Mass Density	91
3.9.1	Density Determined by Mass and Volume Measurement	91
3.9.2	Density Calibration Curve Using CT Numbers.....	92
3.10	Melting Point Measurement	93
CHAPTER 4 RESULTS AND DISCUSSION.....		95
4.1	Determination of Optimal Genipin Gel Compositions for 3D Dosimetry.....	95
4.1.1	Determination of Maximum Visible Absorption Dose Response	95
4.1.1.1	The Optimal Concentration of Genipin.....	95
4.1.2	Melting Point Measurement	104

4.1.2.1	Effect of Gelatin Weight Percent	104
4.1.2.2	Effect of Variation of Sulfuric Acid Concentration	105
4.1.3	Genipin Gel Mass Density.....	106
4.1.4	Temporal Stability Measurements of Genipin Gel Dosimeter	107
4.1.4.1	Pre-irradiation Stability Measurements.....	109
4.1.4.2	Post-irradiation Stability Measurements	111
4.1.5	Reproducibility of Genipin Gel Dosimeter.....	112
4.2	Dosimetric Properties Enhancement of Genipin Gel Using Additives.....	113
4.2.1	Effect of Inorganic Salt on Dosimetric Properties of Genipin Gel.....	114
4.2.2	Effect of Glucose Additives on Dosimetric Properties of Genipin Gel.....	114
4.2.2.1	Effect of Glucose Additives on Mass Density of Genipin Gel	115
4.2.2.2	Effect of Glucose Additives on Melting Point of Genipin Gel	116
4.2.2.3	Effect of Glucose Additives on Genipin Gel Dose Response	117
4.2.3	Effect of AuNPs Additives on Dosimetric Properties of Genipin Gel	119
4.3	Improved the genipin Gel Dosimeters	123
4.3.1	Radiological Properties of Genipin Gel.....	124
4.3.1.1	Calculations of Effective Atomic Number and Electron Density ..	124
4.3.1.2	Linear Attenuation Coefficients	128
4.3.1.3	Density Measurement of Post-Irradiated Gel.....	134
4.4	Dosimetric Characteristics of 6 and 10 MV Therapeutic Photon Beams	136
4.4.1	Calibration Curves of Gel Dosimeters and Radiochromic Film.....	136
4.4.2	Dose Resolution and Uncertainty in Dose Measurement	138
4.4.3	Depth Dose Measurements of genipin and GP-GI-AuNPs Gels	141
4.4.4	Beam Profile Measurements of genipin and GP -GI-AuNPs Gels	144
CHAPTER 5 CONCLUSION AND FUTURE WORK.....		146
5.1	Conclusion	146
5.2	Future work.....	148
REFERENCES.....		150

LIST OF TABLES

TABLE	PAGE
Table 2.1: Characteristics of a typical central axis Depth Dose Curve for Megavoltage Beams	31
Table 2.2: Summary of proposed polymer gel dosimeter	34
Table 2.3: Constituents and formulations of some common PGDs (Schreiner & Olding, 2009).....	37
Table 3.1: The compositions by weight of the polymer gel dosimeters investigated	63
Table 3.2: Tabulated NaI data and calculated photopeak energies	73
Table 3.3: Parameter settings used on all CT imaging experiments	84
Table 4.1: Variations of melting point(T_m) for genipin gel at different weight fractions of gelatin, values are mean \pm SE of mean	104
Table 4.2: Variations of melting point for genipin gel at different concentrations of sulfuric acid, values are mean \pm SE of mean.....	106
Table 4.3: Variations of mass density for genipin gel at different weight fractions of gelatin, values are mean \pm SE of mean.....	107
Table 4.4: Variations of melting point for modified genipin gel at different concentrations of magnesium chloride hexahydrate and potassium chloride ..	114
Table 4.5: Variations of optical dose response of modified genipin gel at different weight fractions of glucose.....	118
Table 4.6: The optical dose responses and the corresponding adjusted correlation coefficients for the linear fits and uncertainties with dose enhancement factors (Ferretti et al.) for genipin gel with and without 10 nm AuNPs (200 ppm) at 6 and 10MV photon energies	122
Table 4.7: Elemental compositions and mass densities list for various materials	124
Table 4.8: Electron density and effective atomic number result for various materials.....	125
Table 4.9: The relative and absolute percent differences list in probability of photons interactions of the two types of gel and water	127
Table 4.10: The percentage error between calculated and evaluated values of electron density for each genipin gel formulations	130
Table 4.11: Comparison calculated value obtained by (XCOM) with experimental value of linear attenuation coefficients (μ) of water at 59.54 keV	130

Table 4.12: The mass attenuation coefficient ratios for each genipin gel formulations compared with that ones for water and muscle	132
Table 4.13: The relative percent differences in the mass attenuation coefficient ratios of both formulation of genipin gel to water and muscle	134
Table 4.14: CT number consistency using the tested materials, list of the mean values of CT_{Ns} with the SE of mean	135
Table 4.15: The variation in gel density upon irradiation were extracted using the density calibration curve.....	135
Table 4.16: The dose and relative dose resolutions of the two genipin gel formulations over the dose range of 15 Gy.....	139
Table 4.17: The tissue–phantom ratio $TPR_{20,10}$ and the absolute percentage difference between the PDDs measurements of GP-GI-AuNPs and IC, EBT3 film and genipin at three different depths	142
Table 4.18: The average decrease in the PDDs values of the fourth dosimeters between 5 and 10 cm depths for both beams energies.....	143
Table 4.19: A comparison of beam cross profile, flatness and symmetry of a 6 and 10 MV photon beams across 50×50 and 100×100 mm ² fields	145

LIST OF FIGURES

FIGURE	PAGE
Figure 0: A diagram of the photoelectric phenomenon (Fosbinder & Orth, 2011).	16
Figure 2.2: The schematic diagram of the coherent scattering (Fosbinder & Orth, 2011).	17
Figure 2.3: Illustrates Compton scattering of an incident x-ray by an outer-shell electron (Fosbinder & Orth, 2011).....	18
Figure 2.4: Pair production occurs with x-ray photons having an energy of 1.02 MeV or greater. Upon interaction with the nuclear force field, the photon disappears and two oppositely charged electrons take its place (Fosbinder & Orth, 2011)	19
Figure 2.5: Components of a typical x-ray tube (Fosbinder & Orth, 2011).....	20
Figure 2.6: Illustrates how the two-production process of x-ray; bremsstrahlung (a) and characteristic x-ray (b).....	23
Figure 2.7: Schematic diagram showing attenuation and transmission of x ray through absorber (Gunderson & Tepper, 2012).....	24
Figure 2.8: The dose profiles of a typical photon beam are characterized by shoulder and toe regions, with definitions for field width, flatness, and penumbra as indicated (Gunderson & Tepper, 2012).....	29
Figure 2.9: A typical photon percent depth dose (PDD) curve is characterized by surface dose, a buildup region, a point of maximum dose, and an exponentially attenuated region (Gunderson & Tepper, 2012).....	30
Figure 3.1: Gel dosimetry involves four major steps: (a) Mix all the gel components by using digital hot plate with magnetic stirrer, after fabrication the gel is poured into calibration vials; (b) Irradiation of gel samples to known doses was performed using 6 and 10 MV photon beams delivered by a dual-energy linear accelerator for calibration and natural isotopes sources for attenuation measurements; (c) the irradiated gel dosimeter samples are scanned with x-ray computerized tomography (x-ray CT) and UV–visible spectrophotometer; (d) finally the data processing tasks.....	61
Figure 3.2: Solid water phantom slabs.....	67
Figure 3.3: A Perspex phantom design for CT scan	68
Figure 3.4: A water phantom design for PDD	69
Figure 3.5: Configurations of Gafchromic®EBT3 film.....	71
Figure 3.6: The medical linear accelerator Siemens PRIMUS™	72

Figure 3.7: Schematically diagram of narrow-beam geometry experiment.....	73
Figure 3.8: NaI linear regression calibration curve using ^{241}Am , ^{226}Ra , ^{137}Cs Sources.....	74
Figure 3.9: Set-up of gel dosimeter samples for irradiation with a medical linac	76
Figure 3.10: The EBT3 film color gradually changes from green to dark green	77
Figure 3.11: Set-up geometry showing EBT3 films in position for irradiation with Clinical Linac	81
Figure 3.12: Samples arrangement in 30 x 30 x 30 cm water tank in different depths.....	82
Figure 3.13: The design of Perspex holder for CT scanning experiments	83
Figure 3.14: CT scanning of the genipin gel at Mount Miriam Cancer Center, Penang, Malaysia, 2014	85
Figure 3.15: Epson Perfection V700 scanner at USM, Penang, Malaysia, 2014.....	86
Figure 3.16: The variation of absorption spectrum of several gel samples at $\lambda_{\text{max}}=601\text{nm}$ in three scales as a function of photons energy	87
Figure 3.17: Calibration curve of mass density with respect to CT numbers	93
Figure 4.1: Variation of the dose response of genipin gels with various genipin concentrations at 25mM of H_2SO_4 and 4% w/w of gelatin, where the solid lines depict linear curves fit over a dose range up to 15 Gy.....	96
Figure 4.2: Variation of dose response ($\text{cm}^{-1}\text{Gy}^{-1}$) with genipin concentration at 25mM of H_2SO_4 and 4% w/w of gelatin.....	97
Figure 4.3: Variation of the dose response of genipin gels with various genipin concentrations at 50mM of H_2SO_4 and 4% w/w of gelatin, where the solid lines depict linear curves fit over a dose range up to 15 Gy.....	98
Figure 4.4: Variation of dose response ($\text{cm}^{-1}\text{Gy}^{-1}$) with genipin concentration while reagent concentrations were sulphuric acid 50mM and gelatin 4.0 % w/w	98
Figure 4.5: The effect of variation concentrations of both genipin and acid at the optical dose response of gel	100
Figure 4.6: Variation of the dose response of genipin gels with various genipin concentrations at 100 mM of H_2SO_4 and 4% w/w of gelatin, where the solid lines depict linear curves fit over a dose range up to 15 Gy.....	101
Figure 4.7: Variation of the dose response of genipin gels with various genipin concentrations at 100mM of H_2SO_4 and 5% w/w of gelatin, where the solid lines depict linear curves fit over a dose range up to 15 Gy.....	102
Figure 4.8: Variation of the dose response of genipin gels with various genipin concentrations at 100mM of H_2SO_4 and 6% w/w of gelatin, where the solid lines depict linear curves fit over a dose range up to 15 Gy.....	102

Figure 4.9: Variation of genipin gel dose response ($\text{cm}^{-1} \text{Gy}^{-1}$) at different weight fractions of gelatin with genipin concentration at 100 mM of sulphuric acid..	103
Figure 4.10: The variation in optical dose response of genipin gel within two different times (6 and 24 hours) after exposure at 6 MV photon beam	107
Figures 4.11: The variation in optical dose response of genipin gel within two different times (6 hours and 24 hours) after exposure at 10 MV photon beam.....	108
Figure 4.12: Pre-irradiation temporal stability of genipin gel dose response within a time period of 14 days at 6 MV photon beam.	110
Figure 4.13: Pre-irradiation temporal stability of genipin gel dose response within a time period of 14 days at 10 MV photon beam.	110
Figure 4.14: Post-irradiation temporal stability of GP gel at 6 and 10 MV photon beams within a time period of 20 days	111
Figure 4.15: The dose response between three equivalent batches scanned within 6 hours post-irradiation	112
Figure 4.16: The dose response between three equivalent batches scanned within 6 hours post-irradiation. Each of the gel batches was prepared within different time intervals and irradiated within 24 hours post-manufacturing	113
Figure 4.17: The effect of glucose weight fractions on the genipin gel mass density	115
Figure 4.18: The effect of glucose weight fractions on the T_m of genipin gel	117
Figure 4.19: The change of absorbance as a function of absorbed dose of genipin gel at different glucose weight fraction.....	118
Figure 4.20: The change of absorbance as a function of absorbed dose of genipin gel irradiated at 6MV photon beam for different concentrations of AuNPs	119
Figure 4.21: The change of absorbance as a function of absorbed dose of genipin gel irradiated at 10MV photon beam for different concentrations of AuNPs	121
Figure 4.22: The photoelectric probability for pure water, genipin gel, and modified genipin gel with 200 ppm of AuNPs	122
Figure 4.23: Fractional probability of photon interaction with water and genipin gels.....	126
Figure 4.24: The probability of photon interaction with water and genipin gels by Compton scatter in two scales as a function of photons energy	126
Figure 4.25: The effective atomic number for each gel formulations comparison with water in three scales as a function of photons energy	128
Figure 4.26: The major photon peak of ^{241}Am point source	129

Figure 4.27: The probability of photon interactions with water as a function of photon energy; the dominant interaction is Compton scattering at these energy regions	129
Figure 4.28: The variation of linear attenuation coefficient of genipin gel with absorbed dose obtained in narrow beam geometry using ²⁴¹ Am point source.....	131
Figure 4.29: The variation of linear attenuation coefficient of GP-GI-AuNPs gel with absorbed dose obtained in narrow beam geometry using ²⁴¹ Am point source .	131
Figure 4.30: Mass attenuation coefficient for water, genipin gel, GP-GI-AuNPs, and muscle at therapeutic energy region	133
Figure 4.31: EBT3 Gafchromic dose response curves for a 6 MV photon beams fitted exponentially with R2=0.9988 (a), a 6 MV photon beam fitted polynomially (second order) with R2=0.9998 (b), a 10 MV proton beam fitted exponentially with R2=0.9985 (c) and a 10 MV proton beam with R2=0.9992 (d)	137
Figure 4.32: The variation in dose resolutions of genipin and GP-GI-AuNPs gels both over the dose range 0 to 15 Gy at photon beams of (a) 6 MV and (b) 10 MV	140
Figure 4.33: The percent depth doses curves of 100 × 100 and 50 x 50 mm ² fields normalized to maximum dose at dmax using 6 and 10 MV photon beams irradiated at 100 cm SSD, (a) 6 MV photon beam of field size 10× 10 mm ² , (b) 10 MV photon beam of field size 100× 100 mm ² , (c) 6 MV photon beam of field size 50× 50 mm ² , (c) 10 MV photon beam of field size 50x50 mm ²	141
Figure 4.34: The beam cross-profile for both beam energies at 10 cm depth, 6 and 10 MV of field sizes 50 × 50 and 100 × 100 mm ² irradiated with 8 Gy, (a) 6 MV photon beam of field size 10× 10 mm ² , (b) 10 MV photon beam of field size 100× 100 mm ² , (c) 6 MV photon beam of field size 50× 50 mm ² , (c) 10 MV photon beam of field size 50x50 mm ²	144

LIST OF ABBREVIATIONS

1D	One dimensional
2D	Two dimensional
3D	Three dimensional
3D–CRT	Three dimensional conformal radiotherapy treatments
AD	Analogue to Digital
ART	Algebraic reconstruction technique
AuNPs	Gold nanoparticles
BANANA	Bis, acrylamide, nitrous oxide and agarose dos
BANG	Bis, acrylamide, nitrogen and aqueous gelatin dosimeter
Bis	N,N'-methylene-bis-acrylamide
CT	Computerized Tomography
DEF	Dose enhancement factor
D_{max}	Maximum absorbed dose
d_{max}	Depth of maximum dose
FOV	Field of view
G	Gelatin
GI	Glucose
GP	Genipin
Gy	Gray
H₂SO₄	Sulfuric acid
IC	Ionizations chamber
ICRP	International Commission on Radiological Protection
IMRT	Intensity-modulated radiation therapy
IR	Ionizations radiation
KeV	Kilo electron Voltage
LET	Linear energy transfer
LINAC	Linear accelerator
MAA	Methacrylic acid
MAG	Methacrylic Acid based Gel
MAGAS	Methacrylic acid, ascorbic acid, gelatin
MAGAT	Methacrylic acid, gelatin and tetrakis
MAGIC	Methacrylic , ascorbic acid in gelatin initiated by copper
MCA	Multichannel Analyzer
MRI	Magnetic Resonance Imaging
MU	Monitor unit
MV	Mega-voltage

NMAG	Normoxic Methacrylic acid based Gel
NMR	Nuclear Magnetic Resonance
NPAG	Normoxic Polyacrylamide Gel
OCT	Optical Computerized Tomography
OD	Optical density
PAG	Polymer acrylamide gel
PAGAS	Polyacrylamide Gel with Ascorbic acid
PAGAT	Polyacrylamide Gel And THPC
PDD	Percentage Depth Dose
PET	Positron Emission Tomography
PGD	Polymer gel dosimeter
ppm	Part per million
QA	Quality and Assurance
ROI	Region of Interest
RPC	Radium Protection Committee
SAD	source-axis distance
SD	Standard deviation
SPECT	Single Photon Emission Computed Tomography
SRS	Stereotactic radiosurgery
SSD	Source-Surface Distance
THP	Tetrakis (hydroxymethyl) phosphonium chloride
THPC	Tetrakis (hydroxymethyl) Phosphonium Chloride
TLD	Thermoluminescent dosimeter
TPS	Treatment Planning System
WHO	World Health Organization

LIST OF SYMBOLS

$wt\%$	Weight fraction
Z	Atomic number
Z_{eff}	Effective atomic number
λ_{max}	Absorption maximum
ρ	Mass density
ρ_e	Electron density
ΔOD	Change in optical density
μ/ρ	Mass attenuation coefficient

LIST OF PUBLICATIONS

Al-Jarrah, A.,Azhar, A.,Iskandar, S.,Abrazak, N. N. A. N.,Ababneh, B.,Tousi, E. T.,
et al. (2014). Effect of Sulfuric Acid Concentration on Radiological
Properties of Genipin Gel Dosimeter. *International Journal of Chemical,
Environmental & Biological Sciences (IJCEBS)*, Volume 2, 136-140.

KAJIAN DOSIMETRI GELATIN GENIPIN: BAHAN KIMIA TAMBAHAN- GEL POLIMER MENGGUNAKAN KEMUDAHAN TERAPEUTIK 6MV DAN 10MV

ABSTRAK

Nanopartikel emas AuNPs dari bahan bernombor atom (Z) tinggi, garam bukan organik dan glukosa telah digunakan dalam kajian ini untuk meningkatkan sifat-sifat fizikal dan radiologi genipin dosimeter gel untuk aplikasi klinikal yang berbeza. Keberkesanan bahan tambah ini telah dikaji untuk respon penyerapan dos yang optimum, ketelusan, takat lebur, ketumpatan, dan kesetaraan air terhadap pengukuran dos secara 3D. Formulasi gel boleh harap yang baharu (GP-GI-AuNPs) telah diformulasi dan dinilai untuk dosimetri 3D menggunakan penilaian optik dan teknik pengimbasan CT untuk bacaan dos. Penambahan glukosa dengan kepekatan optimum 10% (w/w) didapati telah meningkat kestabilan terma gel genipin dan meningkatkan takat lebur (T_m) sebanyak 6°C . Tambahan pula, glukosa membantu melaraskan ketumpatan jisim gel untuk memperoleh sifat-sifat kesetaraan yang dikehendaki. Setitik T_m dan kekuatan gel diperhatikan apabila garam digunakan sebagai bahan tambah. Dengan peningkatan kepekatan garam, kekuatan gel dan T_m menurun. Kesetaraan radiologi air bagi setiap genipin gel dosimeter ditentukan dengan menilai ketumpatan, nombor atom berkesan, dan pekali pengecilan linear. Kesemua nilai dibandingkan dengan nilai air dan otot, membuktikan bahawa sifat radiologi gel baharu adalah menghampiri nilai otot dan boleh dianggap sebagai gel setara air.

Tindak balas maksimum dos optik gel genipin pada foton 6 dan 10 MV adalah masing-masing -0.00526 dan -0.00522 ($\text{cm}^{-1}\text{Gy}^{-1}$). Penambahan AuNPs (kepekatan optimum, 200 ppm), menghasilkan sedikit peningkatan dos optik kurang daripada 10%. Mengikut lengkok kalibrasi ketumpatan yang diperolehi dari pengimbas CT, ketumpatan sampel gel telah diekstrak menggunakan CTNs yang sama. Hasil menunjukkan peningkatan ketumpatan gel lebih kurang mengikut urutan $0.5 \text{ mg cm}^{-3}\text{Gy}^{-1}$ disebabkan oleh penyinaran. Pengiraan resolusi dos juga menunjukkan bahawa gel GP-GI-AuNPs meningkatkan resolusi dos ($\sim 0.05 \text{ Gy}$). Peratus kedalaman dos (PDDs) dan profil dos alur foton 6-MV menggunakan kebuk pengionan (IC), GP-GI-AuNPs, dan filem EBT3 untuk saiz bidang ($100 \times 100 \text{ mm}^2$) dikaji untuk perbandingan dan pengesahan. Berdasarkan keputusan, perbezaan peratusan maksimum mutlak antara ukuran PDD GP-GI-AuNPs dengan IC dan EBT3 filem adalah 4% dan 6%. Kesamarataan IC, GP-GI-AuNPs dan EBT3 filem masing-masing ialah 2.2%, 2.1% dan 1.8%, manakala simetri IC, genipin -GI-AuNPs dan EBT3 filem masing-masing ialah 0.9% 1.0% dan 0.8%. Kajian ini memberi sumbangan yang besar ke arah pembangunan dan kejayaan pelaksanaan dosimetri gel terhadap radioterapi klinikal.

DOSIMETRIC STUDY OF GENIPIN GELATIN-CHEMICAL ADDITIVES POLYMER GEL USING 6 MV AND 10 MV THERAPEUTIC FACILITIES

ABSTRACT

Gold nanoparticles AuNPs of high-Z materials, inorganic salts and glucose have been used in this study to enhance physical and radiological properties of genipin gel dosimeter for different clinical applications. The effectiveness of these additives were investigated for optimum visible absorption dose response, transparency, melting points, density, and water equivalency for 3D dose measurements. A reliable new gel formulation (GP -GI-AuNPs) was formulated and evaluated for 3D dosimetry using optical evaluation and CT scanning techniques for dose readout. The addition of glucose with optimum concentration of 10% (w/w) was found to improve the thermal stability of the genipin gel and increase its melting point (T_m) by 6°C. Furthermore, glucose helps to adjust the gel mass density to obtain the desired tissue-equivalent properties. A drop of T_m and the gel strength were observed when salt was used as additives. As the salt concentration increase, gel strength and T_m decreased. The radiological water equivalence of each genipin gel dosimeters was determined by evaluating the densities, effective atomic numbers, and the linear attenuation coefficients. All of these values were compared with water and muscle values, proving that the radiological properties of the new gel approximate muscle values and could be considered as a water equivalent gel.

The maximum optical dose responses of genipin gel at 6 and 10 MV photon beams were -0.00526 and -0.00522 ($\text{cm}^{-1}\text{Gy}^{-1}$) respectively. The addition of AuNPs (optimum concentration, 200 ppm) has resulted in a slight increment of the optical dose response of less than 10%. According to the density calibration curve obtained from CT scan, the gel sample densities were extracted using the corresponding CTNs. The result displayed an increment of gel density approximately in the order of $0.5 \text{ mg cm}^{-3}\text{Gy}^{-1}$ due to irradiation. The dose resolutions calculations were also indicated that GP–GI–AuNPs gel enhanced dose resolution (~ 0.05 Gy). The percent depth doses (PDDs) and dose profiles of 6 MV photon beams using an ionization chamber (IC), GP–GI–AuNPs, and EBT3 films of field sizes ($100 \times 100 \text{ mm}^2$) were investigated for comparison and verification purpose. According to the results, the maximum absolute percentage difference between the PDD measurements of GP–GI–AuNPs with IC and EBT3 films were 4% and 6%. The flatness of the IC, GP–GI–AuNPs and EBT3 films were 2.2%, 2.1% and 1.8%, respectively, while the symmetry of the IC, GP–GI–AuNPs and EBT3 films were 0.9% 1.0% and 0.8% respectively. This study provides a significant contribution toward the development and successful implementation of gel dosimetry towards clinical radiotherapy.

CHAPTER 1

INTRODUCTION

1.1 Background

Since the discovery of ionizing radiation (IR), x-rays and radioactivity at the end of the 19th century, the biological effects of radiation have been recognized. Its ability to damage cells by producing free radicals and intermediate ions is utilized to induce cell inactivation and death. Subsequently, throughout the 20th century, IR has been introduced as an essential therapeutic tool in clinical oncology. Over the years, several therapeutic techniques, such as intensity-modulated radiotherapy (IMRT), image-guided radiation therapy (IGRT) and intraoperative radiation therapy (IORT) have been proposed to improve the optimal delivery of IR to patients (Bruner et al., 2001; Delaney et al., 2005; Radiation, 2009). At present, accurate dose delivery has significantly improved, allowing more precise deposition of dose in tumors while gradually reducing any unwanted dose to surrounding healthy tissues (Bhide & Nutting, 2010; Begg et al., 2011).

Radiation therapy is the treatment of cancer and other diseases by damaging the genetic material within target cells with IR, in which radiation can be delivered via two modes, namely, externally and internally. In both cases, IR deposits energy as it traverses an absorbing medium can cause damage in target cells or prevent these cells from proliferating and dividing (Feinendegen et al., 2004; Wang et al., 2008). However, cell damage increases with the increase in amount of energy deposited in a mass of tissue, which is termed as absorbed dose (ICRU, 1998). Thus, absorbed dose (D) should be measured in numerous applications. Several effective dosimetry

systems have been developed in the past century. In radiotherapy, dose measurement is of major significance, especially in medical practice. The accurate measurement of the dose imparted to target cells is fundamental in studies of clinical radiotherapy practice, as well as in biological effects of irradiation.

Radiation measurements and the study of radiation effects demand different specifications of the radiation field at the point of concern. Radiation dosimetry deals with methods of quantitatively determining the energy deposited in a given medium by direct or indirect IR (Podgorsak, 2005). Since the inception of IR over a century ago, radiotherapy has become one of the primary tools for treating cancerous cells, with an estimated 50% of all patients who developed cancer requiring radiotherapy at certain phases of their illness (NHMRC, 1996; Begg et al., 2011). Radiotherapy treatment is planned based on the dose required to achieve the clinical objective and the dose constraints of the organs at risk. To optimize the possibility of tumor control, a high dose of radiation to the tumor volume is required (Connell & Hellman, 2009). Major developments have been achieved to address the problem of limited effect on deep-seated tumors because of low penetration in addition to high x-ray dosage delivery.

Besides widening the array of beam energies, technological growth in radiotherapy equipment has also improved tumor targeting while reducing the radiation dose to neighboring healthy tissues. In the past 20 years, numerous sophisticated techniques have been developed, such as the application of electron linear accelerator machines (LINACs) to produce higher-energy x-rays and electron beams in the megavoltage range of energy for radiotherapy (Lind & Brahme, 1995). Enhancement in dose distribution and skin sparing via high-energy x-rays has

improved and continues to increase the effectiveness of radiotherapy in treating cancer, given that tumor cells can be bombarded with a sufficient dose of radiation without causing severe reaction to the skin or adjacent healthy tissues (Bernier et al., 2004).

Dosimetry is a key component of radiotherapy that entails the measurement or calculation of a dose deposited in a given medium, in which dose is the differential energy imparted per unit mass. Dosimetry techniques are used to compare the planned (treatment planning system predicted) dose distribution to the measured dose distribution in a given volume (Schreiner, 2006). For a complex dose distribution, the measurement of the whole dose distribution would be preferential in evaluating whether the dose had been deposited accurately. A radiation dosimeter is a device, instrument, or system that measures or evaluates, either directly or indirectly, the quantity of exposure, absorbed dose or equivalent dose, their time derivatives (rates), or related quantities of IR (Attix, 2008). A dosimeter with its reader is called a dosimetry system. The operating parameters of a radiation dosimeter are dependent on at least one physical property upon which the dosimetric quantity measurement can be based on, and on the accurate calibration of the dosimetry system (Izewska & Rajan, 2005).

To be effective, radiation dosimeters must display certain key features comprising sensitive response to dose, in which sensitivity is independent of dose rate and photon energy, stability over time with high accuracy, and measurement precision. In other words, an ideal dosimeter offers the following main features: a distinctive accuracy and reproducible response that is independent of energy; capability of measuring the dose with a high spatial resolution; a linear response over

a large dynamic range; non-disturbance of the dose to the medium; and the ability to measure the dose distribution in three dimensions. However, not all dosimeters can meet all of these requirements. Thus, the preference for a radiation dosimeter and its reader must be made systematically, taking into consideration the requirements of the measurement conditions (Rosenberg, 2008)

1.2 Motivation for a 3D Dosimeter

Different dosimeters have been used to measure the dose distributions. 3D dosimeters present more advantages over 1D dosimeters, such as ionization chambers (ICs), or 2D dosimeters, such as radiosensitive films, given that the absorbed radiation dose distribution may be recorded in three dimensions based on the type of gel dosimeter utilized. Verifying dose distribution is greatly required in conditions involving intricate dose distributions, such as stereotactic radio-surgery (STR) or intensity-modulated radiotherapy (IMRT). In addition, gel dosimeters may be adapted to become equivalent to soft tissue, and their physical properties may be altered to meet the requirements of certain applications (Ataei, 2012).

The 3D radiation dosimeters are derived from radiation-sensitive materials that undergo transformations in their physical and chemical properties upon irradiation, as a basis for absorbed radiation dose. These transformations, including changes in color, transparency, and density, are measurable (Hurley et al., 2006; Vértés et al., 2010). The response of a model 3D dosimeter is supposed to be firm, explicit, measurable, and reproducible (De Deene, 2004; Baldock et al., 2010). The response should be insensitive to variations in environmental conditions during irradiation and scanning, such as light, humidity, temperature, and pressure.

The response of the 3D dosimeter requires basis on the total radiation dose distribution, but should not be subjective to the radiation dose rate or to the energy transmitted by the radiation beam. However, as radiation delivery techniques increase in complexity, the need for an accurate and practical 3D dosimetry system has increased as an essential requirement for validating dose distributions. In addition, the 3D dosimetry system has undergone a series of developments and improvements (Oldham, 2006). Over the past two decades, several 3D radiation dosimeters have been proposed, among which the Frick gel dosimeter and polymer gel dosimeters are dominant (Gore & Kang, 1984; Maryanski et al., 1994a; Vandecasteele et al., 2011).

In 1984, Gore et al. introduced the Fricke solution, which was initially highlighted by Fricke and Morse (1927), via integrating the solution into a gel matrix as a radiation-sensitive gel that could potentially be used to measure 3D dose distribution (Davies & Baldock, 2008). The Fricke gel dosimeter involves the use of magnetic resonance imaging (MRI) to detect and quantify radiation-induced changes and dose-dependent transformation of ferrous (Fe^{2+}) into ferric (Fe^{3+}) ions in Fricke or ferrous sulfate solutions. Fricke gels have garnered considerable interest as 3D dosimeters given their simple preparation and reproducible results (Schreiner, 2004). However, similar to other conventional gels used in dosimetry, Fricke gels are sensitive to the preparation conditions and procedure, including irradiation and read-outs such as impurities and temperature. Conversely, polymer gel dosimeters comprise water and gelatin, as well as monomers and cross-linkers that polymerize in response to free radicals produced by water radiolysis (Baldock et al., 2010). The amount of cross-linked polymer that forms and precipitates at each site in the gel is dependent on the local radiation dose and the discrete concentration of monomer and

cross-linker. The tightly cross-linked polymer particles developed in the gel modifies the physical properties of the dosimeter. These changes can be detected using MRI, optical computerized tomography (CT), and x-ray CT scans (Maryanski et al., 1993; Jirasek et al., 2010; Olding et al., 2011).

Gel dosimeters are radiosensitive materials that undergo transformations in their chemical configuration upon irradiation, which acts as a basis for absorbed radiation dose. These dosimeters may be recorded the dose distribution in 3D based on the type of gel dosimeter utilized (Jirasek et al., 2009; Rozlan et al., 2011).

1.3 Genipin Gel Dosimeter

Genipin (GP) gel dosimeters are hydrogels infused with a radiation-sensitive material possessing the ability to retain dosimetric information in three dimensions. Over the years, in addition to its use in herbal medicine, genipin has shown more potential distinctive features, such as its biocompatibility and low cytotoxicity (Butler et al., 2003; Fernandes et al., 2013). Genipin radiochromic gel has also exhibited considerable potential as a 3D dosimeter in advanced radiotherapy techniques. Several studies have investigated the characteristics and applications of genipin . Using NMR spectroscopy, Djerassi et al. (1961) analyzed the chemical structure of genipin , which possesses the molecular formula of $C_{11}H_{14}O_5$. genipin has also been cross-linked with amino acid to create stable cross-linked products with dark blue pigments (Lee et al., 2003). Recently, Jordan (2008) introduced the application of genipin gel as 3D dosimeter. Subsequently, various research studies have been conducted to evaluate the application of genipin in radiotherapy applications. For example, Jordan (2009) reported that genipin –gelatin combination presents an adequate response for radioactive dosage up to 50 Gy.

Furthermore, Davies et al. (2013) demonstrated that a genipin –gelatin gel does not diffuse post-irradiation, which is a limiting feature of any gel dosimeter infused with radiation-sensitive species. Instead, the genipin hydrogel is bleached as a monotonic function of dose upon irradiation, and the color change can be optically quantified as an indication of absorbed dose (Cho et al., 2009), thereby facilitating the mapping of absorbed dose distribution in three dimensions with sufficient stability and sensitivity for doses up to 100 Gy (Davies et al., 2010). Furthermore, Davies et al. (2011) asserted that the addition of sulfuric acid increases the sensitivity of genipin gel dosimeter for quality assurance of radiotherapy level dosimetry. This improvement thus ensures the material's potential value as a dosimeter for applications such as the phytosanitary irradiation treatment of food. Gorjiara et al. (2011) studied the water equivalency of genipin by characterizing its radiological properties. Their results indicate that genipin gel exhibits greater water equivalency in comparison with polymer gels and PRESAGE[®] formulation.

1.4 Gold Nanoparticles (AuNPs) in Radiotherapy

AuNPs is notable as one of most efficient and well-studied agents for enhancing radiation dose (Jain et al., 2012). Gold is as an inert material but can be easily mobilized with biocompatible coatings. Although, AuNPs are generally harmless and non-toxic to human, additional studies are needed, given that high doses may definitely be connected to toxicity (Xi et al., 2012). A number of studies have reported that the change of the biocompatible surface and polymer coating lowers the toxicity of AuNPs (Zhang et al., 2008; Kong et al., 2008; Rahman et al., 2009; Liu et al., 2010).

AuNPs were originally classified as potential radiation enhancing agents for *in vivo* computed tomography (CT) imaging by Hainfeld et al. (2014). They concluded that the relatively higher Z number of gold (Au = 79) in contrast to the usually used iodine (I = 53), and its considerably higher absorption coefficient, lead to a 3 times greater contrast per unit weight for gold compared to iodine. AuNPs also demonstrate great potential as contrast agents for imaging functions performed prior to delivery of treatment such as in Image-guided radiation therapy (IGRT) (Jackson et al., 2010; Kim & Jon, 2012). Consequently, treatment supported by AuNPs has added benefits such as the prospect of real-time imaging of targets during and post irradiation; hence, it has the potential to be employed in image-guided radiotherapy.

Based on potential therapeutic applications of AuNPs in radiotherapy, their dose enhancing capabilities have been investigated in several *in vitro* investigations (Sperling et al., 2008; Rahman et al., 2009; Chithrani et al., 2010; Jain et al., 2011). Monte Carlo simulations have also been used to hypothetically simulate and compute the interactions between AuNPs with diverse types of surface treatment techniques and beam energies (Cho, 2005; McMahon et al., 2008; S. X. Zhang et al., 2009). Most of these computational simulations showed that low energy x-rays and gamma-rays are more effective in enhancing radiation doses than the high energy ones.

All above mentioned studies have suggested the increase in photoelectric absorption by high Z materials at kilovoltage photon energies as the rationale supporting AuNPs dose enhancement. Such dose enhancement would not occur at clinically related megavoltage energies, since Z-independent Compton interactions are dominant (Podgorsak, 2010). Despite this, a number of studies have related the

increase in cell death by AuNPs with clinically relevant megavoltage energies (Jain et al., 2011; Tsiamas et al., 2013).

1.5 Problem Statement

The delivery of radiation therapy to tumors is a highly complex and technical medical treatment (Van Dyk, 1999; Khan, 2010). Hence, radiation measurements, investigations of radiation effects, and radiation dosimetry necessitate a range of specifications of the radiation field at the point of interest to determine the energy deposited in a given medium quantitatively, either directly or indirectly, by IR. The use of genipin gel as 3D dosimeter has been effective because of its biocompatibility and low toxicity (Butler et al., 2003; Fernandes et al., 2013). In addition, genipin gel presents high water equivalence and sensitivity for radioactive doses up to 100 Gy (Davies et al., 2010).

However, the material possesses a relatively low melting point of 25 °C (Davies et al., 2013) and requires a long time for imaging. In addition, gel transportation makes genipin susceptible to flaccidity, so the 3D mapping recorded in the gel would be lost (Zhu et al., 2010; Pavoni & Baffa, 2012), which decreases sensitivity to IR. Therefore, this study hypothesizes that increasing the melting point or rigidity of genipin and adjusting its density with the addition of certain chemical components, such as glucose, AuNPs, and inorganic salts, to its original recipe will improve the dosimetric properties of this dosimeter and maintain its dose sensitivity at an acceptable level.

1.6 Significance of Study

In an effort to reduce patient morbidity and increase clinical outcomes, a high demand is placed on the accuracy and precision of dosimetric parameters. Melting point in gel dosimetry is an important factor that affects the validity and capability for 3D dose measurements. This parameter, in particular, is crucial for when the gel melts, resulting in discrepancy of the 3D mapping recorded in the gel (Zhu et al., 2010; Pavoni & Baffa, 2012). Given that the gel melting point of genipin is still below the required level, increasing the melting point will improve its rigidity, transparency, and optical dose response. The feasibility of employing three different chemical additives (inorganic salt, glucose, and gold nanoparticles (AuNPs)) to enhance the dosimetric properties of genipin gel was investigated using optical evaluation and CT scan techniques.

Therefore, attempts will be conducted to enhance the dosimetric properties of genipin gel by means of experimental studies using AuNPs on gel irradiated with 0 Gy to 15 Gy ranges of radiation doses at different concentrations of AuNPs for two energies of external radiation (6 and 10 MV). Glucose will be used to improve the melting point and increase gel rigidity, while AuNPs will be applied to enhance the radiation response of the gel. Two evaluation techniques, namely, optical evaluation and x-ray CT, will be used to verify the 3D radiation dose distributions subsequent to the use of these additives. Improving the melting point will ensure easier integration into the clinical environment.

Furthermore, dose distributions predicted by treatment planning systems (TPS) and dose distribution measured through a phantom require confirmation by accurate dosimetric measurements to be used directly in clinical practice. To achieve

optimal agreement between computed dose distributions by the planning systems and actual delivered dose distributions by a linear accelerator, genipin gels and EBT3 radiochromic films were compared, and IC dosimeter measurements were investigated to verify the capability of genipin gels for determining dose distributions before introduction into clinical practice.

1.7 Objectives of the Study

The overall aim of this study was to enhance certain physical and radiological properties of genipin gel dosimeter by utilizing several chemical additives. The specific objectives of this study are:

1. To fabricate and optimize the concentrations of the different chemical components of genipin gel dosimeters.
2. To assess the effect of chemical additives, namely, AuNPs, inorganic salts and glucose of genipin gel dosimeters.
3. To characterize the genipin gel in therapeutic photon beam and verifying the dosimeter stability.
4. To evaluate the tissue equivalency of genipin gels in terms of dosimetric parameters over a wide energy range of x-ray.

1.8 Scope of Research

This research introduces a new formulation to fabricate low-cytotoxicity gel dosimeter with the capability of mapping the absorbed dose distribution in three dimensions. Typical genipin gel was found to be composed of gelatin as a gelling agent, genipin as a cross-linker, ultrapure water and sulfuric acid. Genipin gel

batches were prepared by varying chemical composition and stored 24 hours at $\sim 4^{\circ}\text{C}$ for gelation. Irradiation of gel samples was performed using 6 and 10 MV photon beams delivered by a dual-energy linear accelerator (LINAC) with Siemens PRIMUSTM LINAC electron beam facility, at Mount Miriam Cancer Center Hospital, Penang, Malaysia. From the onset of the research, the optimal elemental composition of the dosimeter was proposed according to gel rigidity, transparency, radiological properties, and optical dose response. The gels were irradiated to doses up to 20 Gy; the optical dose-response of genipin gel appears to be linear over a dose range up to 15 Gy. Genipin gel dosimeters were read out using x-ray CT and UV–visible spectrophotometer evaluation techniques.

Afterward, the feasibility of employing several chemical additives, namely, AuNPs, inorganic salts and glucose for enhancing the genipin gel dosimetric properties is examined. Moreover, a comparison between genipin gels and EBT3 radiochromic films and ion chamber dosimeter measurements was investigated to verify the capability of genipin gels for determining dose distributions before introduction into clinical practice. However, formaldehyde has been also tested as additive to improve the gel melting point; it didn't show any improvement of genipin gel melting point.

1.9 Thesis Outline

This thesis includes five individual chapters. Chapter one provides a brief introduction to history and development of gel dosimetry; followed by the problem statement, research significance and research objectives. Chapter 2 presents the theoretical background followed by a comprehensive review of the study. It first clarifies the theoretical background of the main interactions of photons with matter,

x-ray production and attenuation. Furthermore, this chapter provides the strengths and limitations of the field of study through a comprehensive review of the literature and identifies the most important backgrounds related to this thesis.

Chapter 3 presents in detail the research methodology involving the experimental procedures of genipin gel dosimetry in terms of materials ,devices and techniques used for fabrication, irradiation and reading out. It also outlines the method of evaluating the gel density, some physical and radiological properties, surface dose, and depth dose profile of the optimal gel formulations.

Chapter 4 entails the results and discussion of all the experiments performed in this study; the optimal gel composition and formulations for maximum visible absorption dose response, the effect of variation of the gel components weight fractions in melting point mass, density, the temporal stability and the reproducibility measurements of genipin gel dosimeter. In addition, the experimental results of the feasibility of employing glucose and AuNPs to enhance genipin gel dosimetric properties. Eventually, Chapter 5 presents the major findings of this thesis, and gives suggestions for future work with regard to this research.

CHAPTER 2

THEORETICAL BACKGROUND AND LITERATURE REVIEW

2.1 Main Interactions of Photons with Matter

Ionizing radiations are classified as direct and indirect. Direct ionizing radiation includes charged particles, such as α and β particles, protons, and electrons that interact with matter mainly by Coulomb forces. Indirect ionizing radiation includes particles with no charge; when interacting with matter, uncharged particles can transfer energy by direct collision with orbital electrons or nuclear interactions, such as, neutron, gamma, and x-rays.

X-ray photons may also be classified according to photon energy. For instance, photons with kinetic energy ranging from 20 keV to 100 keV are superficial or soft X-rays; those with kinetic energies ranging from 200 keV to 400 keV, 400 keV to 800 keV, and $>1,000$ keV are orthovoltage, supervoltage and megavoltage x-rays, respectively (Goldschmidt et al., 1991; Jones, 1994). Studies regarding the interaction of a photon beam with matter have attained a significant importance in science and technology. Precise knowledge of the mechanism by which radiations interact with matter is required to understand diffusion and penetration of radiations in a medium. With advancements in technology, gamma ray, and x-ray spectroscopic techniques, numerous applications in diverse fields, such as medicine, have been developed (Aichinger et al., 2011).

As a photon beam passes through matter, each photon undergoes three possible fates: a photon can penetrate matter without interaction; a photon can be completely absorbed by depositing energy; or a photon can interact with matter and

can be scattered from its original direction and deposit part of its energy (Attix, 2008; Fosbinder & Orth, 2011). As x-rays travel through a patient's tissue, intensity attenuates exponentially because of complete or partial loss of x-ray photon energy; either complete energy loss termed absorption or partial energy loss called scattering may occur (Nikjoo et al., 2012). However, several interaction events are usually involved as x-ray photons interact with tissues; these interactions include photoelectric effect, scattering, and pair production in which Compton scattering is dominant at a therapeutic energy range (Kurudirek & Topcuoglu, 2011). However, a brief description of each interactions mechanism is provided below.

2.1.1 Photoelectric Effect

Photoelectric effect is an electro-quantum phenomenon in which photon energy is absorbed by an orbiting electron of an atom. If photon energy is greater than binding energy of an electron, which differs in various types of matter, this electron is ejected from an atom; such an electron is called a photoelectron that creates a vacancy in a shell; thus, the atom becomes excited after a photoelectron is emitted. The kinetic energy of a photoelectron is calculated using Eq.2.1:

$$E_k = E_0 - E_b \quad (2.1)$$

where E_k , E_0 and E_b are kinetic energy of the photoelectron, the energy of initial input photon, and the electron binding energy, respectively. The photoelectric phenomenon is illustrated in Figure 2.1.

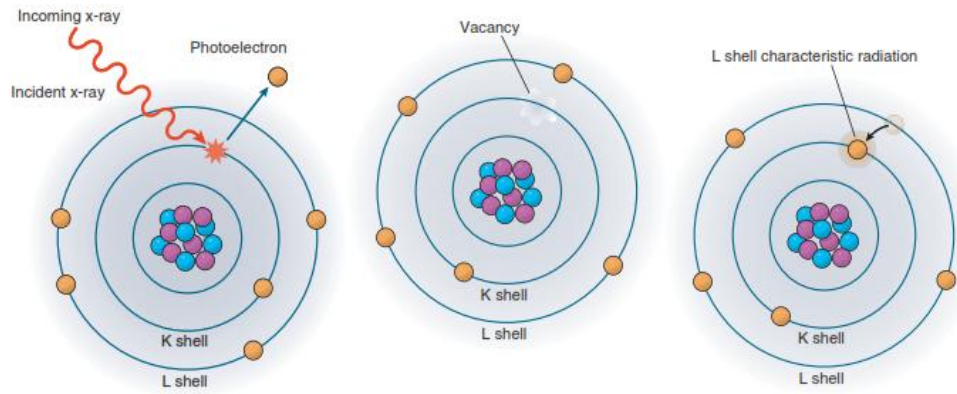


Figure 0: A diagram of the photoelectric phenomenon (Fosbinder & Orth, 2011).

The probability of photoelectric absorption depends on Z of an absorber and photon energy; it is inversely proportional to the cube of photon energy. Therefore, photoelectric effect is significant in photons, such as diagnostic x-rays, with low energy of <100 keV. The proportionality of this interaction is generally expressed as:

$$\tau \propto Z^n (h\nu)^{-3} \quad (2.2)$$

where τ is the probability of the photoelectric effect, Z is the atomic number of the bombarded matter, n is 3 or 4 depending on the energy of the photon, and $h\nu$ is the energy of the primary photon (Saha, 2012)

2.1.2 Rayleigh (Coherent) Scattering

Coherent scattering is the interaction of photons with matter when low-energy photons pass through an element with a high atomic number and change direction without any energy loss and without changing wavelengths before and after interaction occurs. Figure 2.2 shows the schematic of coherent scattering

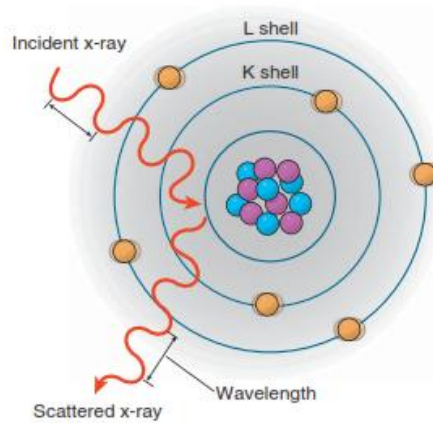


Figure 2.2: The schematic diagram of the coherent scattering (Fosbinder & Orth, 2011).

The coherent scattering is an elastic scattering that also is known as Thompson, classical, or Rayleigh scattering (Hobbie & Roth, 2007; Attix, 2008). This phenomenon occurs primarily at energies <10 keV but is not important in therapeutic and diagnostic radiology.

2.1.3 Compton Scatter (Incoherent Scatter)

In Compton scattering, an x-ray photon loses its energy and changes its direction as this X-ray photon interacts with matter. Therefore, the x-ray wavelength after Compton scattering is greater than that before scattering. Compton scattering equation is expressed as:

$$\lambda' - \lambda = \frac{h}{m_e c} (1 - \cos(\theta)) \quad (2.3)$$

where λ and λ' are the wavelengths of x-ray photons before and after Compton scattering; h , m_e , c , and θ are Planck's constant, electron rest mass, speed of light, and angle of scattered x-ray photons, respectively. The amount of Compton scattering increases as x-ray energy increases. Compton photons can be scattered in

any path not exceeding 180° . Deflection angle is generally controlled by the energy of the initial photon. At a deflection angle of 0° , no energy is transmitted because photon does not vary from the initial direction. As deflection angle increases to 180° , additional energy is provided for the recoil electron, and the energy retained in the scattered photon is reduced. Nonetheless, Compton scattering is usually the main mechanism of a therapeutic array of energies ranging from 100 keV to 1 MeV (Oldham, 2001; Long et al., 2012). A Compton-scattered x-ray photon is characterized by lower energy and longer wavelength than the incident photon (Figure 2.3).

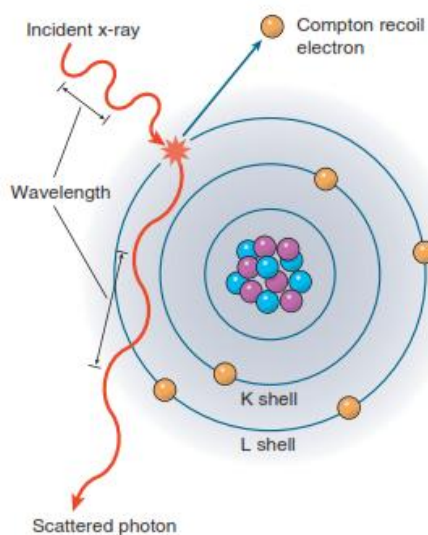


Figure 2.3: Illustrates Compton scattering of an incident x-ray by an outer-shell electron (Fosbinder & Orth, 2011)

2.1.4 Pair Production

For energetic photons of >1 MeV, pair production is the dominant interaction mechanism. Electron rest mass energy is 0.51 MeV; thus, the photon with energy >1.02 MeV can create a pair of electron and positron (anti-mass particle of the

electron) by interacting with the nucleus of an atom (Tavernier, 2010). The photon disappears in the nuclear field of absorber atoms; thus, one electron–positron pair is generated. Figure 2.4 shows a simple schematic of pair production.

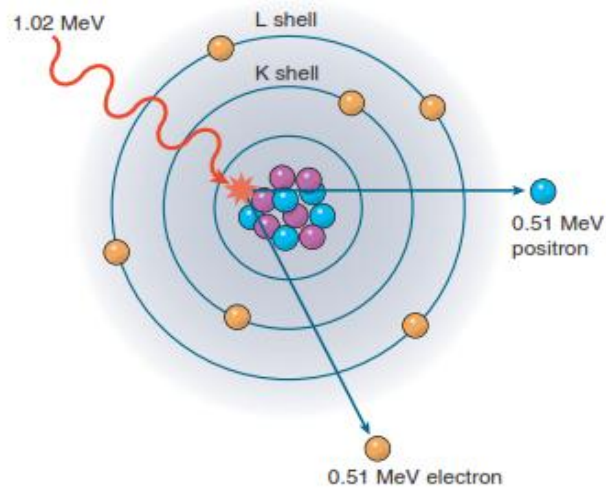


Figure 2.4: Pair production occurs with x-ray photons having an energy of 1.02 MeV or greater. Upon interaction with the nuclear force field, the photon disappears and two oppositely charged electrons take its place (Fosbinder & Orth, 2011)

2.2 Production of X-Rays

In 1895, Wilhelm Röntgen called his newly discovered radiation as x-ray because of its cryptic nature. X-rays are high-energy electromagnetic waves (Hessenbruch, 2002; Slater, 2012). In retrospect, the image of Röntgen’s wife’s left hand was the first published utilization of x-rays. Since this discovery, x-rays have been considerably applied in diagnostic imaging and therapy (Short & Bonner, 1989; Cherry & Duxbury, 2009).

However, x-rays are produced by interactions in atomic shells. In a conventional method, x-ray photons are generated by emission of electrons from a filament (cathode); the emitted electrons are then accelerated with a voltage toward a

metallic target (anode); these electrons subsequently strike the target, thereby converting a small fraction of their kinetic energy into x-ray photons. With these interactions between a target element and electrons, x-ray is produced with different spectra depending on specific elements. In this process, an x-ray device emits two different types of x-ray photons via physical mechanisms: bremsstrahlung and characteristic x-ray (Van Grieken & Markowicz, 2001; Zschornack, 2006; Allisy-Roberts & Williams, 2007).

2.2.1 X-Ray Tubes

A conventional x-ray tube (Figure 05) consists of a partially evacuated glass envelope that contains two electrodes: a negative electrode known as cathode and a positive electrode called anode. The two electrodes are maintained at a sufficient potential difference. The cathode located on one side of the x-ray tube contains a filament; electrons are produced as current is applied on this filament; these electrons then interact with the anode, which contains the focal spot involved in x-ray production, on the opposite side of the x-ray tube (Fosbinder & Orth, 2011; Khan & Gibbons, 2014).

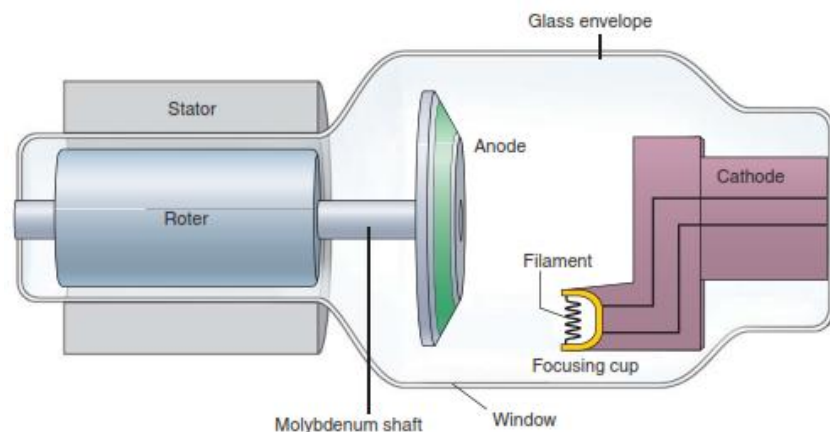


Figure 2.5: Components of a typical x-ray tube (Fosbinder & Orth, 2011)

2.2.2 Characteristic X-Ray Spectrum

Electron transitions between quantized atomic energy levels provide photons with definite wavelengths in visible, UV, and x-ray regions of the electromagnetic spectrum. The energy of these photons is distinct from each atom relative to the binding energy of the target electrons, given that electron binding energies depend on Z (Bushberg & Boone, 2011). Vacancies are created when an incident electron exhibits sufficient energy to eliminate an orbital electron from an inner electron shell; thus, atoms become unstable. Afterward, a high-energy outer-shell electron instantly fills low-energy vacancy that creates a characteristic x-ray photon. This shift in electrons between shells is referred to as characteristic cascade, which can create several x-ray photons for each electron removed from an atom (Beyzadeoglu et al., 2010; Fosbinder & Orth, 2011).

In addition, characteristic x-rays are identified according to the orbital affected by vacancy. For example, radiations stemming from the occurrence of vacancies in K and L shells are referred to as K - and L -characteristic x-rays, respectively. If a vacancy in one shell is filled by an adjacent shell, this vacancy is recognized by a subscript alpha (e.g., $L \rightarrow K$ transition K_α , $M \rightarrow L$ transition L_α). If an electron vacancy is filled by a non-adjacent shell, the subscript beta is used e.g., $M \rightarrow K$ transition K_β) (Hendee & Ritenour, 2003; Bushberg & Boone, 2011; Khan & Gibbons, 2014). The energy of the characteristic x-ray is a measure of the disparity between electron binding energies (E_b) of the respective shells expressed as:

$$E_{(x-ray)} = E_{(b \text{ vacant shell})} - E_{(b \text{ transition shell})} \quad (2.4)$$

2.2.3 Bremsstrahlung Spectrum

In an x-ray tube, a cathode system can accelerate electrons across a vacuum glass tube toward the anode. These electrons then penetrate the anode material by passing close to its atomic nuclei. A coulomb field of these nuclei causes incident electrons to deflect from their initial path. Indeed, in an individual deflection by a target nucleus, incident electrons can radiate different amounts of energy from zero to its total kinetic energy (T) depending on how close it approaches the target nucleus. The energy lost by an incident electron during this encounter appears in the form of an x-ray photon (Dowsett et al., 2006).

Bremsstrahlung (brems) is produced when accelerated electrons are slowed down in different rates by the coulomb field of the anode nuclei. The incident electron must have enough energy to be closed to target nucleus. As a result, the force fields make the electron decelerate or brake and then cause a deflection in the electron directions. According to energy conservation law, an electron loses different amounts of kinetic energy emitted as brems x-ray photon. The amount of lost kinetic energy depends on how close to the nucleus an incident electron is. For instance, more energy is lost when an incident electron is close to the nucleus, producing high-energy brems photon (Fosbinder & Orth, 2011). Consequently, this kind of radiation spectrum is continuous; by contrast, characteristic x-ray spectrum contains sharp spectral lines. Most of the produced x-ray beams exhibit an average energy of approximately one-third to one-half of the maximum energy (Seibert & Boone, 2005). Figure 2.6 illustrates the mechanisms by which bremsstrahlung and characteristic x-rays are produced.

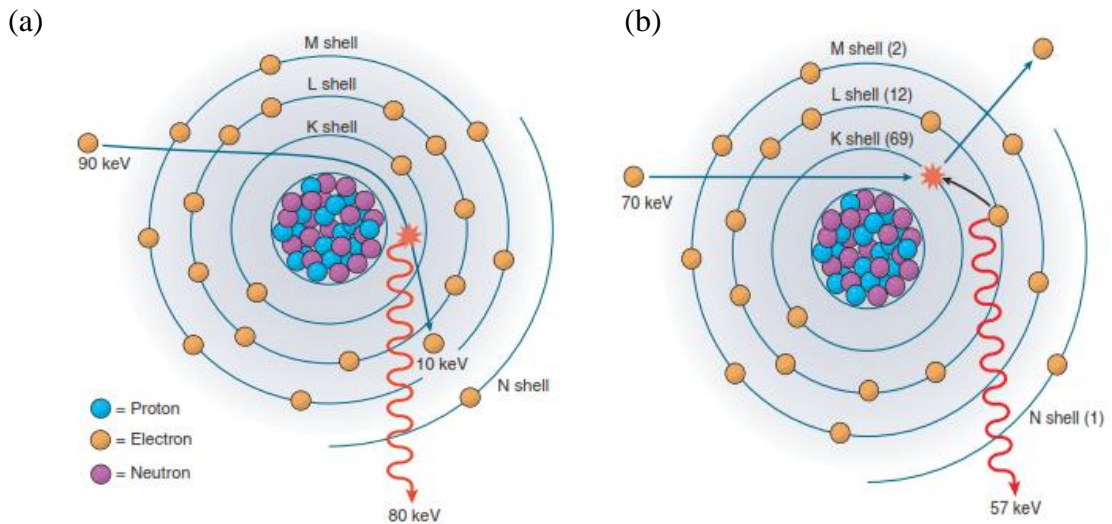


Figure 2.6: Illustrates how the two-production process of x-ray; bremsstrahlung (a) and characteristic x-ray (b)

2.3 X-Ray Attenuation

As an x-ray beam is directed to an absorber, some of the photon beams interact and become completely absorbed or scattered at a large angle from its original path; thus, part of their energy is deposited. Other photon beams completely pass through an absorber without interaction. As a result of either photoelectric or Compton interaction between photons and an absorber, the intensity of an incident photon beam decreases as the beam travels through a certain thickness of the absorber. This loss of photon intensity is called attenuation.

2.3.1 Linear Attenuation Coefficient

For a beam of mono-energetic photons, the intensity of photon beams decreases because of interactions as these photons pass through an attenuator, leading to exponential attenuation; in exponential attenuation, the decrease in beam intensity is determined mainly by thickness, density, and atomic number of the

attenuator (Seegenschmiedt et al., 2009; Powsner et al., 2013). Figure 2.7 illustrates the concept of linear attenuation coefficient (Radiation & (ARPANSA)) according the penetration and intensity reduction of the incident photons beam through an attenuator.

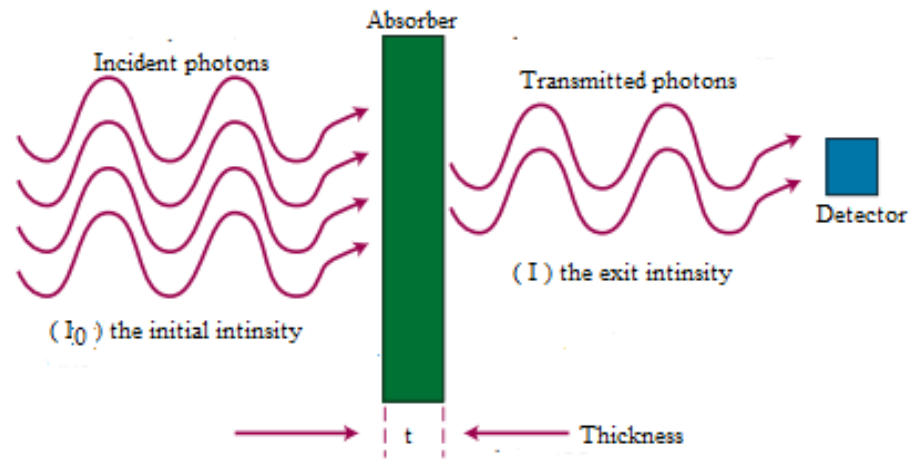


Figure 2.7: Schematic diagram showing attenuation and transmission of x ray through absorber (Gunderson & Tepper, 2012)

If the beam intensity at the exit point of the attenuator is I and the initial intensity of the incident beam is I_0 , then μ is expressed as an exponential function of the thickness t of the attenuator in cm; the intensity of the beam decreases exponentially with the thickness of the absorber, and μ is typically measured in cm^{-1} (Fosbinder & Orth, 2011). Thus, μ may be quantified as:

$$\frac{I}{I_0} = e^{-\mu t} \quad (2.5)$$

μ increases linearly with attenuator density ρ ; therefore, a dense material exhibits great attenuation. For instance:

$$\mu_{\text{water}} > \mu_{\text{ice}} > \mu_{\text{water vapor}}$$